Carborane-Containing Polymer Nanoparticles via Light-Mediated Polymerisation-Induced Self-Assembly

Xinyi Zhang,[1,2] Haoxiang Zeng,[2] Shin Takano,[2] Louis M. Rendina,[1,3*] Markus Müllner[1,2,3*]

[1]School of Chemistry, The University of Sydney, Sydney 2006 NSW, Australia. [2]Key Centre for Polymers and Colloids, School of Chemistry, The University of Sydney, Sydney 2006 NSW, Australia. [3]The University of Sydney Nano Institute (Sydney Nano), The University of Sydney, Sydney 2006 NSW, Australia.

Corresponding authors: markus.muellner@sydney.edu.au; louis.rendina@sydney.edu.au

Table of Contents graph

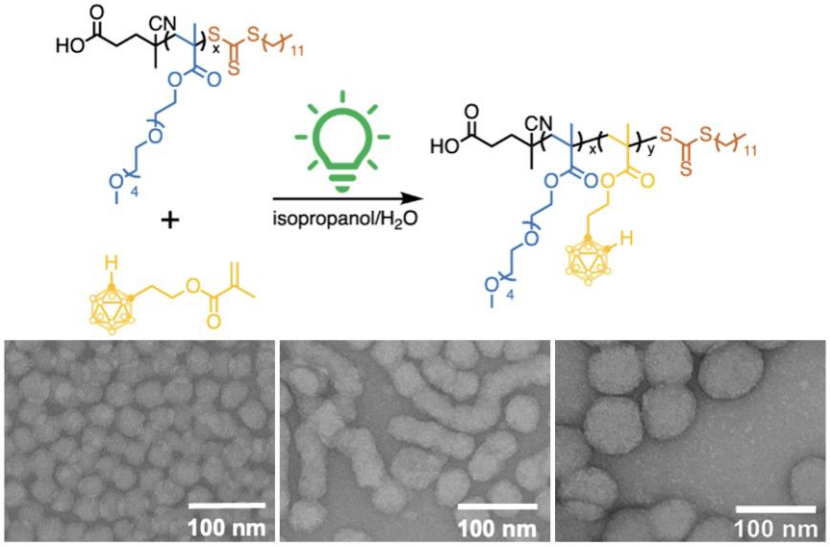

Abstract

Carboranes are an important class of icosahedral carbon-boron clusters that have been intensively studied in the fields of medicinal, organometallic, and materials chemistry. In recent years, there have been efforts to incorporate carboranes into block copolymers to explore their biomedical applications. Few studies have used reversible deactivation radical polymerisation processes to the synthesize carborane-based polymers. In this work, we report the synthesis of a series of well-defined poly[oligo(ethylene glycol) methyl ether methacrylate]-*block*-poly(*closo*-1,2-carboranylethyl methacrylate) (POEGMA-*b*-PCbEMA) block copolymers by means of a photo-mediated reversible addition-fragmentation chain-transfer (RAFT)

polymerisation, and report the formation of nanoparticles of various morphologies through polymerisation-induced self-assembly (PISA). Various parameters including temperature, irradiation source, degree of polymerisation of the core-forming block, solids and water content were found to have an impact on the polymerisation process and the final morphologies.

Introduction

Carboranes are an important class of electron-delocalized, heteroborane clusters comprising of two carbon and ten boron atoms. There are three carborane isomers depending on the position of the two carbon atoms, namely: *closo*-1,2-carborane (*ortho*-carborane), *closo*-1,7-carborane (*meta*-carborane) and *closo*-1,12-carborane (*para*-carborane).[1] Carboranes exhibit interesting properties, including a unique σ-aromaticity, high lipophilicity and hydrophobicity, excellent chemical and metabolic stability, and the ability to form unique 'dihydrogen' bonds (B – H ··· H – X, X = N, O and C.).[2] Additionally, carboranes can be considered inorganic analogues of a rotating phenyl ring or adamantyl cage due to their comparable volumes 140–150 Å^3.[3] To date, carborane cages have attracted great attention as anti-cancer agents,[4] antibiotics[5] and fluorophores.[6,7] Boron neutron capture therapy (BNCT), an experimental binary anti-cancer treatment based on the localised nuclear fission reaction of ^{10}B nucleus upon the capture of a thermal neutron, is one possibility enabled by carboranes due to their high boron content and the very high neutron capture cross section of the naturally-occurring ^{10}B isotope (*ca*. 20% natural abundance).[8–10] However, small carborane compounds suffered from low aqueous solubility, short circulation time and non-specific accumulation *in vivo*.[11] The incorporation of carboranes into nanoparticles is anticipated to overcome some of these challenges and improve their solubility, prolong their circulation time and promote their trans-membrane properties.[12] For potential applications in drug delivery[13] and binary anti-cancer applications,[11,14–16] only a

few carborane-containing block copolymers and their self-assembled materials have been reported to date.

In polymer science, carboranes are mainly incorporated into the polymer backbones by means of polycondensation reactions to enhance the thermal and oxidation stability of polymers such as polyimides, polybenzoxazines and polysilanes, and to tune the emission and absorption properties of fluorescent, conjugated polymers.[3] However, controlled/living radical polymerisation methods including reversible addition-fragmentation chain-transfer (RAFT) polymerisation, atom-transfer radical polymerisation (ATRP) and ring-opening polymerisation (ROP) have only been scarcely used to synthesise carborane-containing block copolymers.[11,14–20] Hence, a limited understanding of the behaviour of carborane-based monomers during such polymerisation processes persists. Notably, in order to prevent possible deboronation reactions of the carborane cages, in particular regarding the most commonly used *closo*-1,2- isomer, *closo*-1,7-carborane derivatives or substituted *closo*-1,2-carborane monomers are generally employed. However, these carboranes are expensive, difficult to source, and feature low to modest overall yields in monomer syntheses (26% - 49%).[11,15,21]

The self-assembly of carborane-containing copolymers to date has only been done via conventional dialysis methods, typically performed at low polymer concentration. The possibility of using polymerisation-induced self-assembly (PISA) to generate copolymers and their corresponding self-assembled structure in one pot has not been studied yet. First applied in the early 2000s, PISA has become a reliable method to prepare polymer self-assemblies *in situ* during polymerisation.[22,23] PISA makes it straightforward to generate dispersions of polymer spheres, worms/rods and polymersomes at scale and in solids contents of up to 50 wt%.[24] Thermal RAFT dispersion polymerisation is the most widely exploited polymerisation strategy for PISA in water,[25] promoting the mobility and flexibility of the core-forming block

and thus facilitating the formation of multiple morphologies. Recently, Boyer's group reported studies on PISA mediated by photoRAFT and photoinduced electron/energy transfer (PET)-RAFT methods, enabling the formation of high-order self-assembly morphologies at room temperature and under an air atmosphere.[26,27] The nanoscale objects formed by a PISA approach have seen increasing exploration and development toward applications in biomedicine, drug delivery, printable polymeric scaffolds, and porous templating materials.[24,28–31]

In this work, we prepared a carboranylethyl methacrylate monomer (CbEMA) from *closo*-1,2-carborane with a high overall yield, and incorporated it into a series of *closo*-1,2-carborane-containing amphiphilic poly[oligo(ethylene glycol) methyl ether methacrylate]-*block*-poly(*closo*-1,2-carboranylethyl methacrylate) (POEGMA-*b*-PCbEMA) diblock copolymers by means of a photoRAFT polymerisation under green LED irradiation using a photo-sensitive 4-cyano-4-[(dodecylsulfanylthiocarbonyl)sulfanyl]-pentanoic acid (CDTPA) chain transfer agent. Using PISA, nano-scale self-assemblies of POEGMA-*b*-PCbEMA with various morphologies were obtained *in situ*. The effects of different experimental parameters on the PISA process were further examined to establish a facile and high yielding synthetic strategy toward carborane-based nanomaterials. The effects of varying the irradiation wavelength, temperature, the DP of the core-forming block, water content and solids content on the system are reported herein.

Results and discussion

Synthesis of monomer and copolymers

The *closo*-1,2-carboranylethyl methacrylate (CbEMA) monomer synthesis was inspired by literature methods.[32,33] *Closo*-1,2-carborane was deprotonated by *n*-butyllithium and reacted

with ethylene oxide in dry THF to give the intermediate carboranyl ethanol (CbE), which was reacted with methacryloyl chloride in the presence of triethylamine in dry DCM to give the required CbEMA monomer (70% yield). Monosubstitution of the carborane was confirmed by ^{1}H NMR spectroscopy for both CbE and CbEMA (**Figures S1 – S6**, Supporting Information).

The macroCTA POEGMA-CDTPA (i.e. stabilizer for the PISA process) was synthesized according to a literature method[27] to avoid potential photodegradation issues stemming of the CDTPA end group.[34,35] The ^{1}H NMR spectrum of the macroCTA POEGMA$_{56}$-CDTPA and its SEC data are shown in the Supporting Information (**Figures S7** and **S8)**. Test polymerizations on the CbEMA monomer were carried out using CDTPA in both conventional thermal RAFT polymerisation on a hot plate and photo-initiated RAFT polymerisation in a photo reactor (**Figure S9**, Supporting Information). (N.B.: because the LED strip generated heat during irradiation, the temperature of the photoRAFT polymerization was set to either 28 °C or 48 °C with/without a portable electric fan.) The thermal RAFT polymerisation was carried out at 80 °C under N_2 in the presence of AIBN in toluene, whereas the photoRAFT polymerisation was carried out in an Ar glovebox at 48 °C using green LED without using any external radical sources. The DP of the homopolymers were different, however this was not considered to affect the polymerisation properties of the monomer. As a result, the green light irradiated photo polymerisation was found to give a better yield (93%) within a shorter period (6 h) at a lower temperature (48 °C) while maintaining a good level of controllability (Đ = 1.23) of the polymerisation process, as compared to the thermal method (conversion 71%, reaction time 22 h, Đ = 1.12). The SEC traces of both homopolymers are shown in **Figure S10**. Notably, the reactions were found to be extremely sensitive to air, and an argon atmosphere was found to be effective in maintaining the repeatability and high yields of the reactions. Thus, a CDTPA-mediated photoRAFT polymerisation method in an Ar glovebox was chosen for the following PISA study. A typical PCbEMA ^{1}H NMR spectrum is shown in **Figure 1**.

In addition, since carborane is known to be highly thermally stable, the decomposition temperature (T_d, where 5% weight loss was observed) and glass transition temperature (T_g) were measured for the homopolymer $PCbEMA_{93}$ by thermogravimetric analysis (TGA) and differential scanning calorimetry (DSC) under N_2. The T_d was 282 °C and T_g was *ca.* 140°C (**Figures S11**, **S12**, Supporting Information), which were higher than those of the phenyl analogues poly(2-phenylethyl methacrylate) (PPEMA, T_g = 42 °C)[36] and poly(benzyl methacrylate) (PBzMA, T_g = 54 – 60 °C).[37]

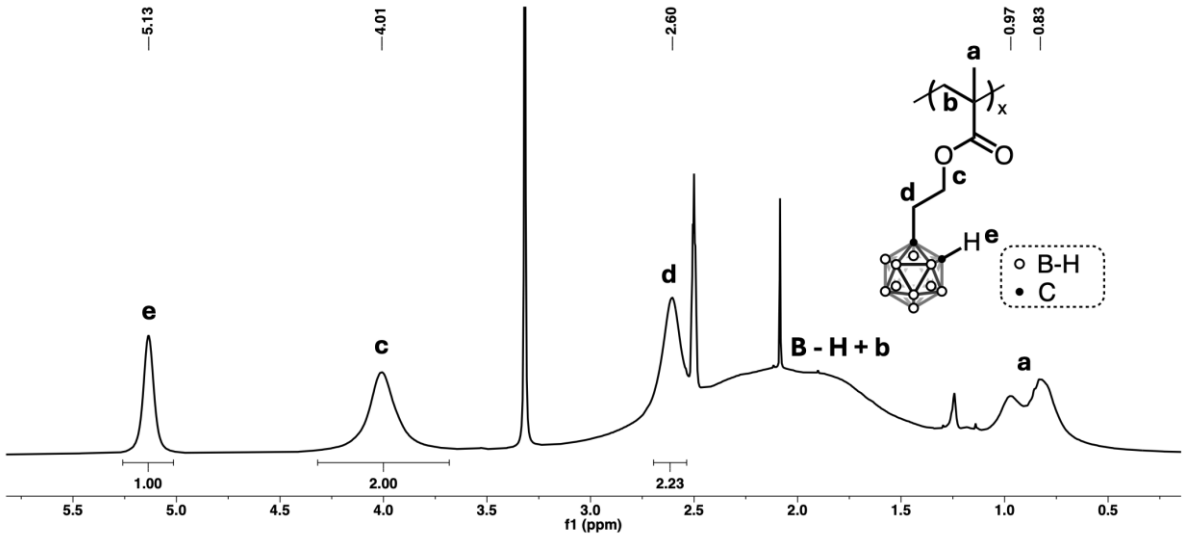

Figure 1. ^{1}H NMR spectrum of the homopolymer $PCbEMA_{93}$ (DMSO-d_6, 500MHz, 298K).

PISA process of POEGMA-*b*-PCbEMA mediated by photoRAFT polymerisation

An appropriate solvent system is key to a successful PISA process, in which all starting materials dissolve adequately while the resulting core-forming block dissolves poorly to facilitate micellar nucleation.[24] To determine the ideal solvent system for POEGMA-*b*-PCbEMA PISA process, methanol, ethanol, isopropanol, aqueous/alcohol solution and DMSO/aqueous solution were chosen based on the relative solubility of each component. As a result, only a mixed isopropanol/aqueous solution gave a satisfactory final reaction mixture

without phase separation (data not shown). Notably, unlike its phenyl analogue BzMA which went through PISA process in ethanol,[27] the existence of water in this solvent was found to be crucial for the successful formation of POEGMA-*b*-PCbEMA self-assemblies. While 10 *v/v*% water content gave only polymer precipitates, a higher water content (30 *v/v*%) was found to produce less interconnected self-assemblies (**Figure 2**) with larger dispersity in SEC (**Table 1**). This trend of the core-forming block PCbEMA to form more compact individual cores as water content increased can be explained by the high hydrophobicity of the carborane cage. To balance between the successful formation of nanoscale self-assemblies and their interconnectivity, the final water content was chosen to be 20 *v/v*%. Thus, the chain extension of the hydrophobic PCbEMA block was carried out in an 80/20 *v/v*% isopropanol/water solution at [M]:[macroCTA] = 250:1 for kinetic studies. Key peaks in the ^{1}H NMR spectrum of POEGMA-*b*-PCbEMA are shown in **Figure 3a**. A clear MW shift toward higher molecular weight was confirmed by SEC (**Figure 3b**).

Table 1. Synthesis and characterization of $POEGMA_{50}$-*b*-$PCbEMA_{100}$ polymers and nanoparticles prepared at water contents of 10 *v/v*%, 20 *v/v*% and 30 *v/v*%.

Polymer Composition[a]	Water content[b]	Conversion[a]	$M_{n,\,NMR}$ (g/mol)[a]	$Đ_{SEC}$[c]	$Size_{DLS}$ (nm)[d]	PDI_{DLS}[d]	TEM[e]
$POEGMA_{50}$-$PCbEMA_{94}$	10%	94%	39 700	1.12	-	-	-
$POEGMA_{50}$-$PCbEMA_{92}$	20%	92%	39 200	1.21	404	0.23	mixed
$POEGMA_{50}$-$PCbEMA_{93}$	30%	93%	39 400	1.30	75	0.08	spheres

[a] Determined based on NMR (DMSO-d_6, 300MHz, 300K) integrations; [b] refers to the volume ratio (*v/v*) of water in isopropanol/water solutions; [c] measured in DMAc at 298K, calibrated with PMMA standards; [d] sizes by number calculated by DLS; [e] description of phases was based on the TEM images.

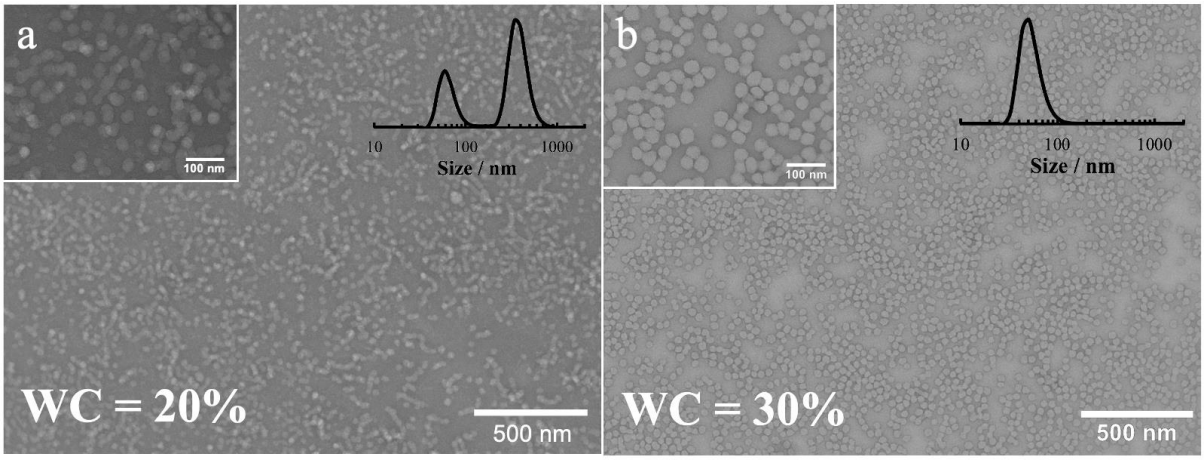

Figure 2. TEM micrographs of $POEGMA_{50}$-*b*-$PCbEMA_{100}$ nanoparticles formed at water contents of a) 20 *v/v*% and b) 30 *v/v*%. Insets show the number-weighted DLS sizes distribution.

Kinetics study

Kinetics studies were conducted under green and blue LEDs at both 28 °C and 48 °C using a $POEGMA_{56}$-CDTPA macroCTA ($M_{n,\ NMR}$ = 15400 g/mol, Đ = 1.14). The chain extension process of a $POEGMA_{56}$-*b*-$PCbEMA_{250}$ was studied, and the reaction rate, reaction control and the self-assembly properties were compared in order to optimize the reaction conditions (**Figures 3c-e**).

First-order kinetics were observed for green LED irradiated reactions at both 28 °C and 48 °C (**Figure 3d**). Compared to a reported PISA study for POEGMA-*b*-PBzMA,[27] the $POEGMA_{56}$-*b*-PCbEMA system exhibited comparable high conversions within a much shorter reaction time with no apparent inhibition periods, while maintaining a satisfactory control over the chain propagation process at the same time. At 28 °C, the conversion of the reaction reached 95% after 18 hours which was 25% faster than the POEGMA-*b*-PBzMA system (which required 25 h), whereas a conversion of 93% was achieved within only 6 hours at 48 °C (**Figure 3c**). Under both conditions, the dispersity (Đ) generally stayed below 1.35, although a growing trend with the chain extension was observed (**Figure 3e**). This trend was also observed in other light-driven RAFT-mediated PISA process,[26,27] which could be an indication of gradual end group degradation upon irradiation during the photoRAFT polymerisation. The high dispersity observed at 18 h in the green light/28 °C reaction was likely due to the CTA photodegradation and the inefficiency of the stabilizer block when DP_{PCbEMA} was above 200, which will be discussed later. TEM images confirmed that both reactions gave a mixture of individual nanospheres and strings of interconnected nanospheres which were evenly sized (*ca.* 50 nm) (**Figure 4a, 4b**).

On the other hand, the use of a blue LED led to a drastic increase in reaction rate, where the reaction reached a conversion of 93% within 3 hours without an obvious inhibition period (**Figure 3b**). However, like the POEGMA-*b*-PBzMA system,[27] the reaction showed high Đ between 1.3 and 1.5 during the chain propagation and two-stage kinetics (**Figure 3d, 3e**), where an apparent drop in the reaction rate was observed after the conversion had reached 50%. This was likely due to the fast formation of a rigid hydrophobic core that was hard for monomers to penetrate. The SEC trace of the blue light reaction showed a much higher ratio (*ca*. 20%) of dead macro-CTA chains compared to green light irradiated reactions (**Figure S13**, Supporting Information) which can be explained by the higher rate of photodegradation of the trithiocarbonate end group under the more energetic blue LED light, as reported in literature.[38] The TEM showed mainly individual nanospheres sized *ca.*70 nm (**Figure 4c**). Thus, for the remainder of this study, we focused on green LEDs.

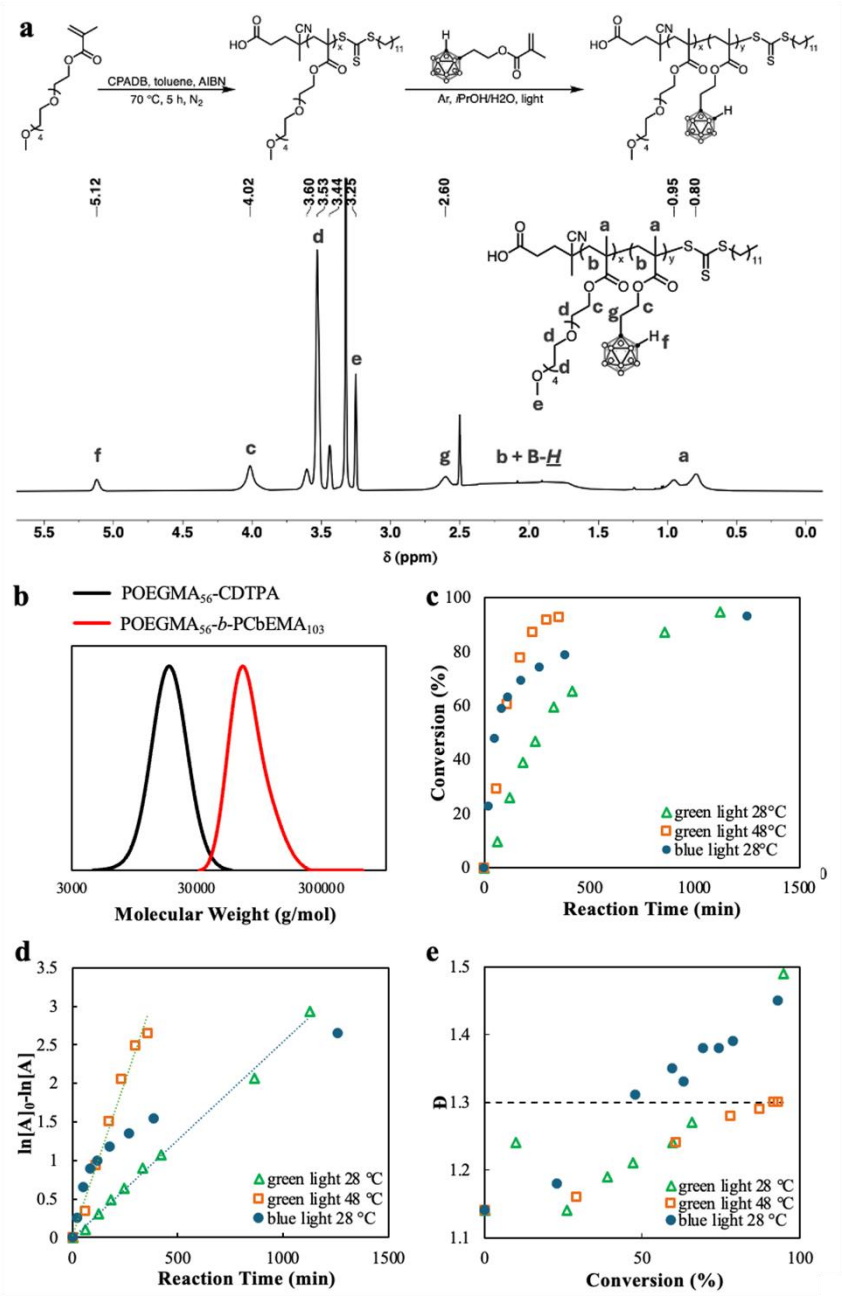

Figure 3. a) Scheme of the PISA reaction and the ^{1}H NMR spectrum of the block copolymer POEGMA-*b*-PCbEMA. b) Molecular weight shift of block copolymer pOEGMA$_{56}$-pCbEMA$_{100}$ as compared to pOEGMA$_{56}$ macroCTA. c) – e) Kinetics study of the PISA process of pOEGMA$_{56}$-pCbEMA$_{250}$ under green/blue LED light at 28/48 °C.

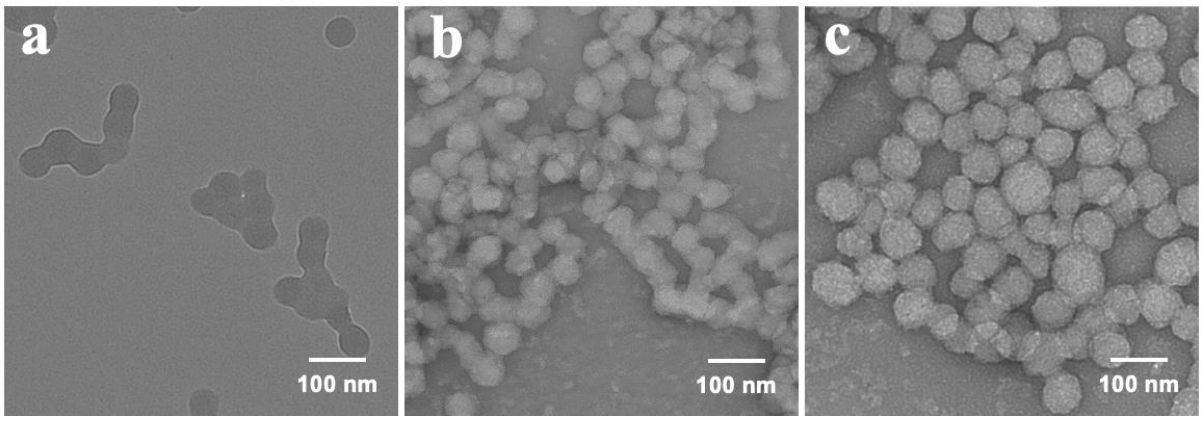

Figure 4. TEM images of POEGMA$_{56}$-*b*-PCbEMA$_{250}$ nanoparticles obtained from kinetic studies under a) green LED light at 28 °C, b) green LED light at 48 °C and c) blue LED light at 28 °C. Histogram of Figure 4c is shown in the Supporting information Figure S14.

In order to obtain a thorough understanding of the morphology evolution, a series of PISA experiments were carried out on the POEGMA-*b*-PCbEMA system with different DP_{PCbEMA} and solids content. The effect of reaction temperature was also evaluated.

Effect of DP_{PCbEMA} on the PISA process of POEGMA-*b*-PCbEMA. To study the effect of DP_{PCbEMA} on the PISA process of POEGMA-*b*-PCbEMA block copolymer system, a series of POEGMA$_{56}$-*b*-PCbEMA$_x$ (x = 50 – 300) polymers were synthesized by chain extending POEGMA$_{56}$-CDTPA macroCTA ($M_{n,NMR}$ = 17200 g/mol, D = 1.13) with CbEMA monomer under Ar at 48 °C in a mixture of 80/20 *v/v*% isopropanol/water solution (**Table 2**). High conversions above 94% were confirmed by ^{1}H NMR measurements. A good control over propagation process, with DP_{PCbEMA} between 50 and 200, was confirmed by SEC (unimodal traces with Đ = 1.06 – 1.32, **Figure S15**, Supporting Information), although an increase in dispersity was observed with the growth of DP_{PCbEMA}, which was also reported in other PISA studies initiated by light.[26,27] However, when DP_{PCbEMA} reached 300, a multimodal SEC trace and a high dispersity of 1.75 were observed, which indicated that DP_{PCbEMA} should be limited to 200.

Visually, the turbidity of the final reaction mixtures of the nanoparticles increased with the DP_{PCbEMA}, while the viscosity peaked at DP_{PCbEMA} 150 (tested by inverting the reaction vials),

at which point a translucent gel was formed (**Figure S16**, Supporting Information). Despite the high T_g of the core forming PCbEMA block, TEM images confirmed a morphological evolution from spheres, short rods/strings of interconnected spheres, large spherical aggregates, to finally large irregular aggregates for the $POEGMA_{56}$-*b*-$PCbEMA_x$ system (**Figure 5a-e**). The nanoparticle size increased with DP_{PCbEMA}, and the diameter of each spherical unit grew from *ca.* 25 nm to more than 100 nm. The interconnectivity of the nanospheres was found to be in good accordance with the viscosity of the final reaction mixture: from DP_{PCbEMA} 50 to DP_{PCbEMA} 150, the viscosity of the final reaction mixtures increased as the nanoparticles became more interconnected, both peaked at DP_{PCbEMA} 150; at DP_{PCbEMA} 200 and 300, the small nanoparticles packed into individual larger aggregates and, accordingly, a dramatic decrease in the viscosity of the reaction mixtures was observed, as both reaction mixtures were free-flowing fluids.

The same series of $POEGMA_{56}$-*b*-$PCbEMA_x$ (x = 50 – 300) syntheses were also carried out at ambient temperature (28 °C) while the reaction time was extended to 18 hours. SEC results showed comparable polymerization control to the one at a higher temperature (48 °C) before (**Figure S17**, Supporting Information). A similar morphology evolution was seen in TEM images. Although the same morphologies appeared at larger DP_{PCbEMA} at 28 °C compared to that at 48°C, and the size of each spherical unit was slightly smaller at the same DP_{PCbEMA}, which could be explained by the lower flexibility of the core at the lower temperature hindering the fusion of the cores (**Figure 5f-j**). Interestingly, a much higher interconnectivity between the spherical units started to form at DP_{PCbEMA} as low as 100, and a much larger DP_{PCbEMA} range (x = 100 - 300) wherein gels were formed at the end of the reaction (**Figure S18**, Supporting Information). The results once again demonstrated that higher thermal energy boosted reaction kinetics but led to a reduced nanoparticle interconnectivity.

Additionally, to elucidate the structure of the spherical nanoparticles, small-angle X-ray scattering (SAXS) and wide-angle X-ray scattering (WAXS) were carried out on the $POEGMA_{56}$-*b*-$POEGMA_{48}$ suspension (**Figure S19**, **S20**). A concentration-dependent scattering profile was observed in SAXS measurements. The interparticle interaction at an interval of *ca*. 35 nm occurred at a concentration of 6.0 wt%, which corresponded to the particle size. A core-shell structure was determined as the extrapolated scattering profile could be reproduced using Pedersen's polymer micelle model.[39] No crystalline packing of the core was found according to WAXS measurements.

Table 2. Synthesis and characterization of $POEGMA_{56}$-*b*-$PCbEMA_x$ (x = 50 - 300) polymers and nanoparticles prepared at a solids content of 30%.

Entry	Polymer Composition[a]	Temperature (°C)	Conversion[a]	$M_{n,\,NMR}$ (g/mol)[a]	$Đ_{SEC}$[b]	$Size_{DLS}$ (nm)[c]	PDI_{DLS}[c]
1	$POEGMA_{56}$-$PCbEMA_{48}$		95%	29 600	1.05	29	0.21
2	$POEGMA_{56}$-$PCbEMA_{103}$		92%	43 800	1.13	41	0.14
3	$POEGMA_{56}$-$PCbEMA_{144}$	28	95%	54 400	1.17	110	0.13
4	$POEGMA_{56}$-$PCbEMA_{213}$		97%	72 200	1.40	283	0.18
5	$POEGMA_{56}$-$PCbEMA_{299}$		96%	94 400	1.70	370	0.18
6	$POEGMA_{56}$-$PCbEMA_{57}$		96%	31 900	1.06	82	0.14
7	$POEGMA_{56}$-$PCbEMA_{109}$		96%	45 300	1.13	124	0.15
8	$POEGMA_{56}$-$PCbEMA_{167}$	48	96%	60 300	1.23	200	0.24
9	$POEGMA_{56}$-$PCbEMA_{208}$		94%	70 900	1.32	160	0.19
10	$POEGMA_{56}$-$PCbEMA_{318}$		94%	99 300	1.75	223	0.05

[a] Determined based on NMR (DMSO-d_6, 300MHz, 300K) integrations; [b] measured in DMAc at 298K, calibrated with PMMA standards; [c] sizes by number calculated by DLS.

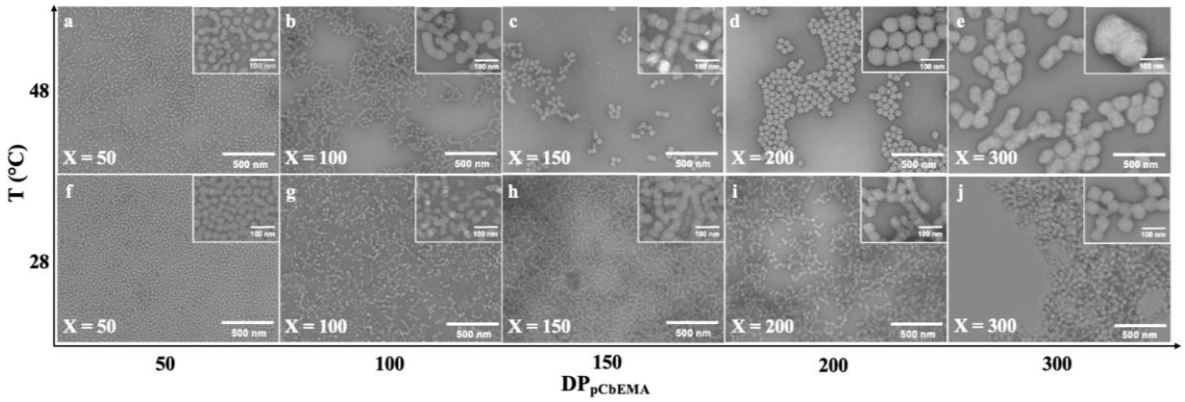

Figure 5. TEM images of $POEGMA_{56}$-*b*-$PCbEMA_x$ (x = 50, 100, 150, 200 and 300) nanoparticles formed at 48 °C (a - e) and 28 °C (f - j), 30 wt% in 80/20 *v/v*% isopropanol/water under green light (nanoparticles were stained by 2% uranyl acetate). Histograms of Figure 5d and 5f are shown in the Supporting information Figure S14.

Effect of solids content on the PISA process of POEGMA$_{56}$-*b*-PCbEMA$_{100}$. In order to further understand the morphology evolution, photoRAFT polymerisations were carried out for POEGMA$_{56}$-*b*-PCbEMA$_{100}$ at a range of solids contents (SC) from 0.15 to 0.40 at 48 °C (**Table 3**). The chain extension of CbEMA from POEGMA$_{56}$-CDTPA macroCTA was performed under green light and an Ar atmosphere. All reactions exhibited high conversions (> 90%) and low dispersity (Đ < 1.15) based on NMR and SEC results, respectively (**Figure S21**, Supporting Information). TEM images demonstrated a clear trend in the morphology evolution (**Figure 6**). At lower solids contents (SC = 0.15 and 0.20), the self-assemblies were individual nanospheres, while an arrangement occurred at SC = 0.20 where the nanospheres aligned along curved lines, which was a transitional phase before fusion/interconnection happened at SC = 0.25, 0.30 and 0.35 to form short nanorods and longer strings of nanospheres. At high SC = 0.40, large nanospheres and a small amount of interconnected large spherical dimers were formed. Once again, the viscosity (tested by inverting the reaction vials) corresponded with the relative interconnectivity of the self-assemblies, with viscous fluids forming at SC = 0.15 and 0.20 when the self-assemblies were individual nanospheres, and gels forming at SC = 0.25, 0.30, 0.35 and 0.40 when interconnected nanoparticles were present (**Figure S22**, Supporting Information).

Table 3. Synthesis and characterization of POEGMA$_{56}$-*b*-PCbEMA$_{100}$ copolymers and nanoparticles prepared at 48 °C at different solids contents.

Entry	Polymer Composition[a]	Solids Content	Conversion[a]	$M_{n,\,NMR}$ (g/mol)[a]	$Đ_{SEC}$[b]	$Size_{DLS}$ (nm)[c]	PDI_{DLS}[c]
11	POEGMA$_{56}$-PCbEMA$_{105}$	15%	91%	44 300	1.09	50	0.09
12	POEGMA$_{56}$-PCbEMA$_{107}$	20%	93%	44 800	1.10	53	0.08
13	POEGMA$_{56}$-PCbEMA$_{104}$	25%	90%	44 100	1.12	86	0.15
14	POEGMA$_{56}$-PCbEMA$_{109}$	30%	96%	45 300	1.13	124	0.15
15	POEGMA$_{56}$-PCbEMA$_{115}$	35%	98%	46 900	1.12	92	0.13
16	POEGMA$_{56}$-PCbEMA$_{95}$	40%	92%	41 700	1.11	354	0.11

[a] Determined based on NMR (DMSO-d_6, 300MHz, 300K) integrations; [b] measured in DMAc at 298K, calibrated with PMMA standards; [c] sizes by number calculated by DLS.

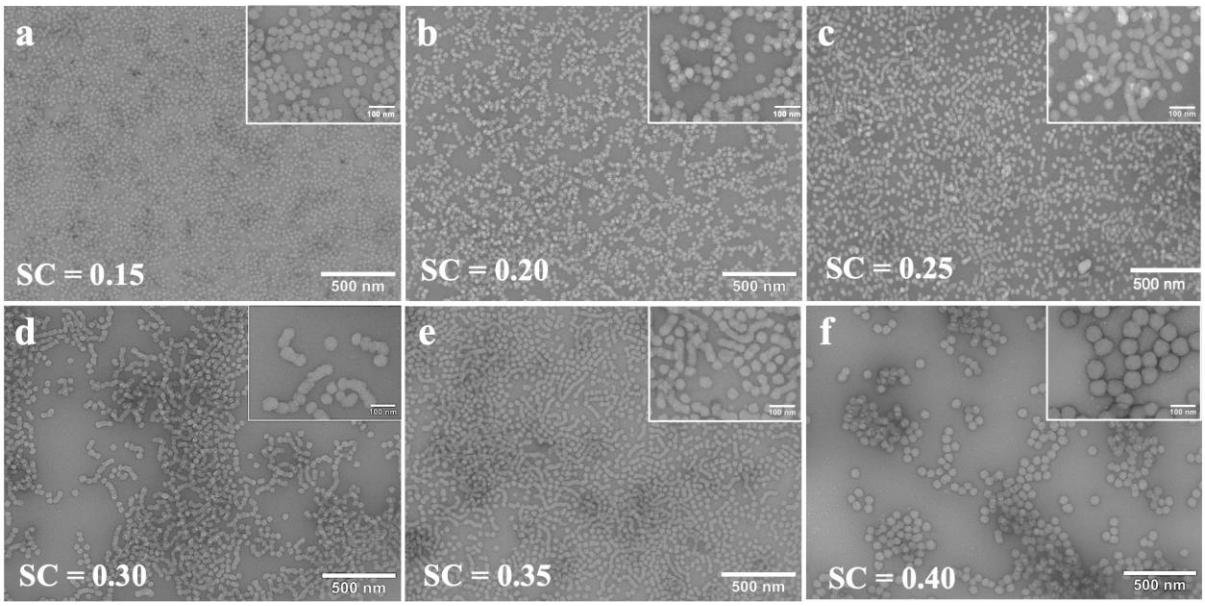

Figure 6. TEM images of POEGMA$_{56}$-*b*-PCbEMA$_{100}$ nanoparticles formed at different solids content (SC = 0.15, 0.20, 0.25, 0.30, 0.35 and 0.40) at 48 °C in 80/20 *v/v*% isopropanol/water under green light. Histograms of Figure 6a, 6b and 6f are shown in the Supporting information Figure S14.

In all systems, no evidence of uniform nanoworms or vesicle morphologies was observed. Although a low degree of core fusion was observed in the formation of short nanorods in this study, it was thought that the core flexibility was not high enough to support further rearrangement of the self-assembly structures at temperatures lower than 50 °C due to the high T_g of the core-forming PCbEMA. However, slow core fusion was indeed observed for POEGMA$_{56}$-*b*-PCbEMA$_{150}$ in a dilute dispersion (0.4 mg/ml) in 80/20 *v/v*% isopropanol/water after 7 days of storage at 0 °C (**Figure S23**, Supporting Information). Besides, the opportunities to achieve conventional higher order morphologies are likely possible if further fine tuning of the reaction conditions occur, such as the addition of a plasticizer or a co-monomer.

Conclusions

We synthesized a carboranylethyl methacrylate monomer and employed photoRAFT-mediated PISA to synthesize amphiphilic carborane-containing POEGMA-*b*-PCbEMA block copolymers and their corresponding nano-scale self-assemblies. PCbEMA homopolymer and POEGMA-*b*-PCbEMA block copolymers could be efficiently synthesized *via* green light-

driven RAFT polymerisation with low dispersity and high conversions compared to thermal RAFT polymerisation. An investigation of the effects of DP_{PCbEMA}, temperature, and solids content on the polymerisation process and morphology evolution of the self-assemblies underscored the reliable formation of carborane-containing nanospheres, short nanorods, interconnected strings of nanospheres and large nanoscale aggregates. The viscosity and gelation of the reaction mixture could be used as a reference to determine the interconnectivity of the nanoparticles. With a better understanding of the properties and behaviors of carboranes in polymers and self-assemblies, the potential of carboranes in polymer science can be further explored. Overall, our study highlights a straightforward nanoparticles fabrication method with high carborane loading. As carboranes can be useful agents in BNCT, our nanomaterials fabrication may prove useful for future biomedical applications.[3]

Experimental Section

Materials and Methods

Closo-1,2-carborane was purchased from Boron Specialties LLC (US), and all the other reagents were commercially available from Sigma-Aldrich and Merck. Methacryloyl chloride was distilled before use. Poly(ethylene glycol) methyl ether methacrylate (M_n 300) was filtered through basic alumina before use. THF and DCM were dried over 4Å molecular sieves for 2 days before use. Other reagents were used as received. Column chromatography was performed with silica gel 60 LR, 0.04-0.06 mm from Chem-Supply. Thin layer chromatography (TLC) was performed on TLC silica gel 60 F254 aluminium plates from Merck. Carborane-containing small molecules were visualised using an acidified $PdCl_2$ (1%) aqueous staining solution upon heating. The LED strip Tapo L930 was purchased from TP-link, the peak wavelengths of green LED and blue LED are 515 nm and 460 nm, respectively, with a fluctuation range of 5 nm.

NMR spectroscopy

^{1}H, $^{13}C\{^{1}H\}$ and $^{11}B\{^{1}H\}$ NMR spectra were recorded using Bruker Avance 300 MHz and 500MHz spectrometers at 300 K. Small molecules were measured in $CDCl_3$ (Cambridge Isotopes) and polymers were measured in DMSO-d_6 (Sigma-Aldrich).

Size Exclusion Chromatography (SEC)

SEC measurements were performed using a UFLC Shimadzu Prominence SEC system equipped with 5 μm, 10^4 Å and 10^5 Å Phenogel^{TM} columns calibrated with PMMA standards. The eluent was dimethylacetamide (DMAc) containing LiBr (0.03 *wt*%) and BHT (each at 0.05 *wt*%) running at a flow rate of 1 ml/min at 50 ºC. The samples were filtered through a 0.45 μm nylon syringe filter before injection. $M_{n,\,SEC}$ was only used to show the molecular weight shift of the carborane-containing polymers, the exact numbers were not useful due to the huge difference between carborane-containing polymers and the PMMA standard.

Dynamic Light Scattering (DLS)

DLS measurements were performed in 1.5 mL semi-micro polystyrene cuvettes, using a Malvern Zetasizer Nano ZS equipped with a He-Ne 633 nm laser at a scattering angle of 173°.

Transmission electron microscopy (TEM)

TEM was performed on a JEM-2100CR instrument equipped with a 5k × 4k CMOS camera (EMSIS). Images were collected in bright-field mode with a spot size of 3 at an accelerating voltage of 200 kV. Diffraction contrast enhanced by using an objective lens with a 20 μm aperture. TEM sample preparation was as described below: All self-assemblies were dispersed in an 80/20 v/v isopropanol/water solution and stirred overnight. 4 μL of the polymer self-assembly solution was dropped onto a carbon-coated copper grid and dried in air for 60 seconds.

The remained solution was blotted by a filter paper. The samples were negatively stained by 2% uranyl acetate (UA) solution for 30 seconds, blotted and dried in air before imaging.

Thermogravimetric analysis (TGA)

TGA measurements were performed on a TA Instruments Discovery thermogravimetric analyser and analysed using a TA Instruments Trios software. 0.93 mg of dried polymer sample was loaded onto a 100 μL platinum plate and heated up to 700 °C at 10 °C/min in N_2 at a flow rate of 20 mL/min.

Differential scanning calorimetry (DSC)

DSC measurements were performed on a Mettler Toledo DSC823e Differential Scanning Calorimeter and analysed using a STARe software. 1.9 mg of dried polymer sample was loaded onto a 40 μL aluminium holder and heated from 25 °C to 250 °C at 10 K/min in N_2 at a flow rate of 50 ml/min. The temperature was held at 250 °C for 30 min in the first cycle to remove the residual traces of solvent and data was collected in the second cycle.

Small-angle X-ray scattering (SAXS) and Wide-angle X-ray scattering (WAXS)

Small-angle X-ray scattering and wide-angle X-ray scattering measurements were carried out on a SAXSpoint 5.0 instrument (Anton Paar, UK) at an incident beam wavelength of 0.154 nm. The digital detector was placed 556.95 mm from the samples for SAXS experiments, and 116.47 mm from the samples for WAXS experiments. The X-ray transmittance of a sample was determined using the equipped transmittance detractor. SAXS and WAXS samples were diluted directly from the final reaction mixture using the same isopropanol/water 80/20 *v/v* solution. A series of dispersions with concentrations of 0.3 wt%, 0.6 wt%, 1.5 wt% and 6.0 wt% were measured in SAXS. WAXS was done on a 6.0 wt% nanoparticle dispersion.

Synthetic Methods

The synthesis of carboranylethanol (1)

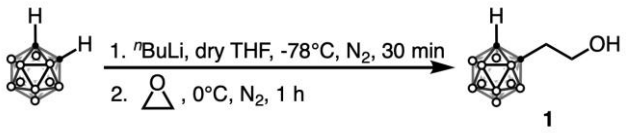

n-Butyllithium (1.6 M in hexane, 1.25 ml, 2 mmol) was added dropwise to a solution of *closo*-1,2-carborane (288.5 mg, 2 mmol) in dry THF (6 ml) under N_2 at -78ºC with stirring. After 30 minutes, ethylene oxide (2.5 - 3.3 M in THF, 1.08 ml, 2.7 mmol) was added dropwise to the mixture. Then the reaction was stirred at 0ºC for another hour before quenched with saturated NH_4Cl aqueous solution (2 mL). The mixture was extracted with ethyl acetate (3 mL x 3). The organic phase was combined, dried over Na_2SO_4 and concentrated *in vacuo*. Purification by silica gel column chromatography (petroleum benzine : ethyl acetate = 5:1 *v/v*) and freeze drying afforded **1** as a colourless solid (298 mg, 1.56 mmol, 78.2%). ^{1}H NMR (500MHz, $CDCl_3$) δ (ppm): 3.97 (s, 1H), 3.80 (t, 2H), 2.91-1.50 (br m, 10H), 2.50 (t, 2H); $^{13}C\{^1H\}$ NMR (500MHz, $CDCl_3$) δ (ppm): 73.11, 60.85, 60.51, 39.93; $^{11}B\{^1H\}$ NMR (500MHz, $CDCl_3$) δ (ppm): -2.09 (s, 1B), -5.37 (s, 1B), -9.47 (s, 2B), -10.96 (s, 2B), -12.08 (s, 2B), -12.85 (s, 2B).

The synthesis of carboranylethyl methacrylate (2)

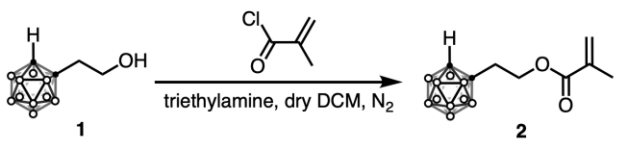

Methacryloyl chloride (195.4 μL, 2.0 mmol) was added dropwise to a solution of **1** (380.9 mg, 2.0 mmol) and triethylamine (348.5 μL, 2.5 mmol) in dry DCM (1 mL) under N_2 at 0ºC with stirring. Then the reaction was warmed to room temperature and stirred overnight. The mixture was washed 3 times with brine and the organic phase was dried over Na_2SO_4 and concentrated

in vacuo. Purification by silica gel column chromatography (petroleum benzine/DCM = 1:1 *v/v*) afforded **2** as a viscous, colourless liquid (477 mg, 1.85 mmol, 92.3%). ^{1}H NMR (500MHz, $CDCl_3$) δ (ppm): 6.10 (s, 1H), 5.63 (s, 1H), 4.25 (t, 2H), 3.66 (s, 1H), 3.40-1.20 (br m, 10H), 2.63 (t, 2H), 1.94 (s, 3H); ^{13}C{^{1}H} NMR (500MHz, $CDCl_3$) δ (ppm): 166.81, 135.74, 126.76, 72.20, 62.08, 60.90, 36.87, 18.37; ^{11}B{^{1}H} NMR (500MHz, $CDCl_3$) δ (ppm): -1.98 (s, 1B), -5.19 (s, 1B), -9.09 (s, 2B), -11.19 (s, 2B), -12.12 (s, 2B), -12.90 (s, 2B).

The synthesis of PCbEMA-CDTPA homopolymer

PCbEMA-CDTPA homopolymer was synthesized via either thermal RAFT polymerisation or photoRAFT polymerisation.

Thermal RAFT method:

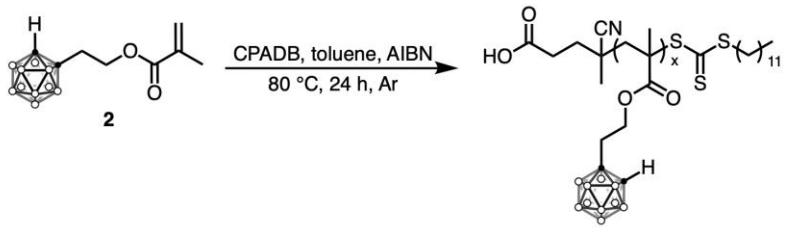

CbEMA (98.1 mg, 0.38 mmol), CDTPA (1.40 mg, 0.0035 mmol), AIBN (0.113 mg, 0.00069 mmol) and toluene (0.31 mL) were added into a 5 mL Schlenk tube and degassed by 3 cycles of freeze-pump-thaw. The reaction mixture was heated at 80 ºC for 22 h and quenched by exposure to air. After precipitation into diethyl ether 3 times and freeze drying, a colourless, glassy solid was obtained. DMAc SEC using PMMA standard indicated Đ = 1.12. A conversion of 71.1% was calculated based on the ^{1}H NMR integrations of the C_{cage}–H proton and the alkenyl proton ($\alpha = (1 - \frac{\int I_{=CH}^{6.09 - 6.06\ ppm}}{\int I_{C_{cage}\text{-}H}^{5.25 - 5.03\ ppm}}) \times 100\%$), and thus the calculated MW of the homopolymer was determined to be $M_{n,\,mCTA} = MW_{CDTPA} + \alpha \times \frac{[CbEMA]_0}{[CDTPA]_0} \times MW_{CbEMA} = 20509.17$ g/mol.

photoRAFT method:

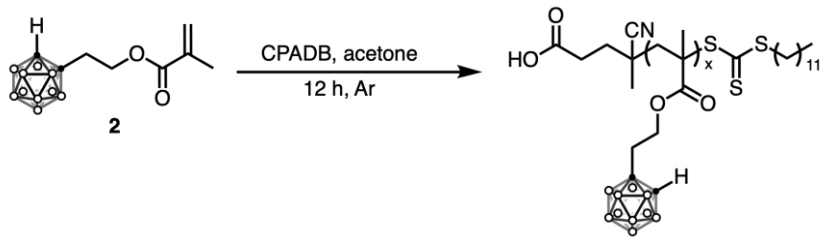

CbEMA (189.0 g, 0.73 mmol), CDTPA (2.65 mg, 0.0066 mmol), and acetone (0.66 mL) were added into a 2 mL vial and purged with Ar for 15 min in an ice bath. The mixture was irradiated by green LED in an Ar glovebox overnight and quenched by exposing to air. After dialysis against acetone and drying at 50 °C under a N_2 flow overnight, a light-yellow solid was obtained. DMAc SEC using PMMA standard indicated Đ = 1.23. A conversion of 93.1% was calculated based on the ^{1}H NMR integrations of the C_{cage}–H proton and the alkenyl proton ($\alpha = (1 - \frac{\int I_{=CH}^{6.09 - 6.06\ ppm}}{\int I_{C_{cage}\text{-}H}^{5.25 - 5.03\ ppm}}) \times 100\%$), and thus the calculated MW of the homopolymer was determined to be $M_{n,\,mCTA} = MW_{CDTPA} + \alpha \times \frac{[CbEMA]_0}{[CDTPA]_0} \times MW_{CbEMA} = 27178.42$ g/mol.

The synthesis of POEGMA-CDTPA macroCTA

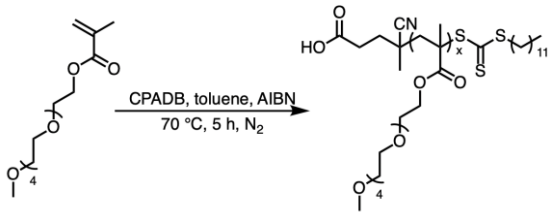

POEGMA-CDTPA macroCTA was synthesized according to literature.[27] OEGMA (3.0 g, 10.0 mmol), CDTPA (40.4 mg, 0.1 mmol), AIBN (3.3 mg, 0.02 mmol) and toluene (10 mL) were added into a well-sealed 25 mL round bottom flask and purged with N_2 for 30 min in an ice bath. The mixture was heated at 75 °C for 5 h and quenched by exposure to air. Precipitation into 50 mL cold diethyl ether 3 times afforded a bright-yellow, sticky liquid. DMAc SEC using

PMMA standard indicated $M_{n,\ SEC}$ = 18300 g/mol, Đ = 1.13. A conversion of 55.5% was calculated based on the ^{1}H NMR integrations of the alkene proton =C-H at T = 5 h and T = 0 h using toluene peaks as the reference (conv. = $\frac{\int I^{6.10\text{-}6.01\ ppm}_{=CH,\ T=5h} / \int I^{7.57\text{-}6.84\ ppm}_{tol.,\ T=5h}}{\int I^{6.10\text{-}6.01\ ppm}_{=CH,\ T=0h} / \int I^{7.57\text{-}6.84\ ppm}_{tol.,\ T=0h}}$), and thus the calculated MW of the macroCTA was determined to be $M_{n,\ mCTA} = MW_{CDTPA} + conv. \times \frac{[OEGMA]_0}{[CDTPA]_0} \times MW_{OEGMA}$ = 17503.67 g/mol.

General procedure of POEGMA-*b*-PCbEMA photo-RAFT mediated PISA

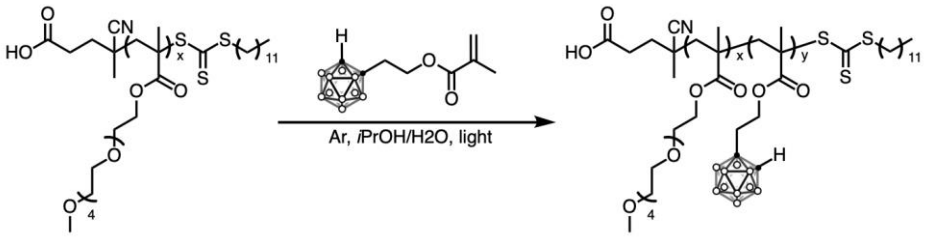

A typical photoRAFT-mediated PISA reaction of [**2**]:[mCTA]=100:1 with 30 *wt*% solids content at 28 °C under green light was set up as follows: **2** (104.7 mg, 0.405 mmol), mCTA (60.0 mg, 4.05 × 10^{-3} mmol), *i*PrOH (370.9 μL, 291.5 mg) and deionized water (92.7 μL, 92.7 mg) were added to a 2 mL vial and degassed by Ar for 15 min in an ice bath before irradiation with green LED light in an Ar glovebox. After 18 h, the reaction was quenched by exposure to air. Precipitation into 50 mL cold diethyl ether 3 times afforded a white solid. The conversion was determined using ^{1}H NMR based on the ratio of the integrations of the alkenyl proton =C-H and C_{cage}-H, where the initial ratio at T = 0 h was 1 (conv. = $\int I^{6.10\text{-}6.01\ ppm}_{=CH,\ T} / \int I^{5.22\text{-}5.04\ ppm}_{C_{cage}H,\ T}$).

Supporting Information

Supporting results, including monomer and polymer characterisations (NMR, SEC, differential scanning calorimetry – DSC), electron microscopy and x-Ray scattering.

Author Contributions

M. M. conceived the idea and co-supervised the research with L. M. R. X. Z. planned and developed the experimental setup and performed all the experiments and analysed the data. H.

Z. and S. T. performed the TEM measurements. S. T. performed the X-ray scattering experiments. All the authors discussed the results. X. Z. co-wrote the manuscript with input from all the authors. The authors declare no conflict of interest.

Acknowledgments

This research was facilitated by access to Sydney Analytical, a core research facility at the University of Sydney. The authors acknowledge the technical and scientific assistance from Sydney Microscopy & Microanalysis, The University of Sydney node of Microscopy Australia and Sydney Cytometry. The authors thank the Key Centre for Polymers and Colloids (KCPC) for access to equipment. M.M. acknowledges the Australian Research Council for a Future Fellowship (FT200100185) and Discovery Project (DP220100452), respectively. M.M. is a grateful recipient of a University of Sydney Research Accelerator (SOAR) Prize.

References

(1) Grimes, R. N. Icosahedral Carboranes. In *Carboranes*; Elsevier, 2016; pp 283–502. https://doi.org/10.1016/B978-0-12-801894-1.00009-3.

(2) Fanfrlík, J.; Lepšík, M.; Horinek, D.; Havlas, Z.; Hobza, P. Interaction of Carboranes with Biomolecules: Formation of Dihydrogen Bonds. *ChemPhysChem* **2006**, *7* (5), 1100–1105. https://doi.org/10.1002/cphc.200500648.

(3) Zhang, X.; Rendina, L. M.; Müllner, M. Carborane-Containing Polymers: Synthesis, Properties, and Applications. *ACS Polymers Au* **2024**, *4* (1), 7–33. https://doi.org/10.1021/acspolymersau.3c00030.

(4) Marfavi, A.; Kavianpour, P.; Rendina, L. M. Carboranes in Drug Discovery, Chemical Biology and Molecular Imaging. *Nat Rev Chem* **2022**, *6* (7), 486–504. https://doi.org/10.1038/s41570-022-00400-x.

(5) Fink, K.; Uchman, M. Boron Cluster Compounds as New Chemical Leads for Antimicrobial Therapy. *Coord Chem Rev* **2021**, *431*, 213684. https://doi.org/10.1016/j.ccr.2020.213684.

(6) Yamamoto, H.; Ochi, J.; Yuhara, K.; Tanaka, K.; Chujo, Y. Switching between Intramolecular Charge Transfer and Excimer Emissions in Solids Based on Aryl-Modified Ethynyl–o-Carboranes. *Cell Rep Phys Sci* **2022**, *3* (2). https://doi.org/10.1016/j.xcrp.2022.100758.

(7) Marfavi, A.; Yeo, J. H.; Leslie, K. G.; New, E. J.; Rendina, L. M. New Boron-Based Coumarin Fluorophores for Bioimaging Applications. *Aust J Chem* **2022**, *75* (9), 716–724. https://doi.org/10.1071/CH21320.

(8) Alberti, D.; Michelotti, A.; Lanfranco, A.; Protti, N.; Altieri, S.; Deagostino, A.; Geninatti Crich, S. In Vitro and in Vivo BNCT Investigations Using a Carborane Containing Sulfonamide Targeting CAIX Epitopes on Malignant Pleural Mesothelioma and Breast Cancer Cells. *Sci Rep* **2020**, *10* (1). https://doi.org/10.1038/s41598-020-76370-1.

(9) Calabrese, G.; Daou, A.; Barbu, E.; Tsibouklis, J. Towards Carborane-Functionalised Structures for the Treatment of Brain Cancer. *Drug Discov Today* **2018**, *23* (1), 63–75. https://doi.org/10.1016/j.drudis.2017.08.009.

(10) Chen, Y.; Du, F.; Tang, L.; Xu, J.; Zhao, Y.; Wu, X.; Li, M.; Shen, J.; Wen, Q.; Cho, C. H.; Xiao, Z. Carboranes as Unique Pharmacophores in Antitumor Medicinal Chemistry. *Mol Ther Oncolytics* **2022**, *24*, 400–416. https://doi.org/10.1016/j.omto.2022.01.005.

(11) Ruan, Z.; Liu, L.; Fu, L.; Xing, T.; Yan, L. An Amphiphilic Block Copolymer Conjugated with Carborane and a NIR Fluorescent Probe for Potential Imaging-Guided BNCT Therapy. *Polym Chem* **2016**, *7* (26), 4411–4418. https://doi.org/10.1039/c6py00799f.

(12) Mitchell, M. J.; Billingsley, M. M.; Haley, R. M.; Wechsler, M. E.; Peppas, N. A.; Langer, R. Engineering Precision Nanoparticles for Drug Delivery. *Nat Rev Drug Discov* **2021**, *20* (2), 101–124. https://doi.org/10.1038/s41573-020-0090-8.

(13) Xiong, H.; Zhou, D.; Qi, Y.; Zhang, Z.; Xie, Z.; Chen, X.; Jing, X.; Meng, F.; Huang, Y. Doxorubicin-Loaded Carborane-Conjugated Polymeric Nanoparticles as Delivery System for Combination Cancer Therapy. *Biomacromolecules* **2015**, *16* (12), 3980–3988. https://doi.org/10.1021/acs.biomac.5b01311.

(14) Xiong, H.; Wei, X.; Zhou, D.; Qi, Y.; Xie, Z.; Chen, X.; Jing, X.; Huang, Y. Amphiphilic Polycarbonates from Carborane-Installed Cyclic Carbonates as Potential Agents for Boron Neutron Capture Therapy. *Bioconjug Chem* **2016**, *27* (9), 2214–2223. https://doi.org/10.1021/acs.bioconjchem.6b00454.

(15) Ruan, Z.; Yuan, P.; Liu, L.; Xing, T.; Yan, L. Carborane and Cyanine Conjugated Galactose Targeted Amphiphilic Copolymers for Potential near Infrared Imaging-Guided Boron Neutron Capture Therapy (BNCT). *International Journal of Polymeric Materials and Polymeric Biomaterials* **2018**, *67* (12), 720–726. https://doi.org/10.1080/00914037.2017.1376199.
(16) Ruan, Z.; Yuan, P.; Jing, T.; Xing, T.; Yan, L. PH-Sensitive Polypeptide Conjugated with Carborane Clusters and Cyanine for NIR Bioimaging and Multi-Therapies. *Macromol Res* **2018**, *26* (3), 270–277. https://doi.org/10.1007/s13233-018-6034-z.
(17) Simon, Y. C.; Ohm, C.; Zimny, M. J.; Coughlin, E. B. Amphiphilic Carborane-Containing Diblock Copolymers. *Macromolecules* **2007**, *40* (16), 5628–5630. https://doi.org/10.1021/ma0709093.
(18) Simon, Y. C.; Coughlin, E. B. Ring-Opening Metathesis Copolymerization of Cyclooctene and a Carborane-Containing Oxanorbornene. *J Polym Sci A Polym Chem* **2010**, *48* (12), 2557–2563. https://doi.org/10.1002/pola.24032.
(19) Kahraman, G.; Wang, D. Y.; von Irmer, J.; Gallei, M.; Hey-Hawkins, E.; Eren, T. Synthesis and Characterization of Phosphorusand Carborane-Containing Polyoxanorbornene Block Copolymers. *Polymers (Basel)* **2019**, *11* (4). https://doi.org/10.3390/polym11040613.
(20) Fernandez-Alvarez, R.; Hlavatovičová, E.; Rodzeń, K.; Strachota, A.; Kereïche, S.; Matějíček, P.; Cabrera-González, J.; Núñez, R.; Uchman, M. Synthesis and Self-Assembly of a Carborane-Containing ABC Triblock Terpolymer: Morphology Control on a Dual-Stimuli Responsive System. *Polym Chem* **2019**, *10* (22), 2774–2780. https://doi.org/10.1039/c9py00518h.
(21) Gratton, S. E. A.; Parrott, M. C.; Adronov, A. Preparation of Carborane-Containing Polymers by Atom Transfer Radical Polymerization. *J Inorg Organomet Polym Mater* **2005**, *15* (4), 469–475. https://doi.org/10.1007/s10904-006-9000-8.
(22) Cornel, E. J.; Jiang, J.; Chen, S.; Du, J. Principles and Characteristics of Polymerization-Induced Self-Assembly with Various Polymerization Techniques. *CCS Chemistry* **2021**, *3* (4), 2104–2125. https://doi.org/10.31635/ccschem.020.202000470.
(23) Cunningham, V. J.; Alswieleh, A. M.; Thompson, K. L.; Williams, M.; Leggett, G. J.; Armes, S. P.; Musa, O. M. Poly(Glycerol Monomethacrylate)-Poly(Benzyl Methacrylate) Diblock Copolymer Nanoparticles via RAFT Emulsion Polymerization: Synthesis, Characterization, and Interfacial Activity. *Macromolecules* **2014**, *47* (16), 5613–5623. https://doi.org/10.1021/ma501140h.
(24) D'Agosto, F.; Rieger, J.; Lansalot, M. RAFT-Mediated Polymerization-Induced Self-Assembly. *Angew. Chem. Int. Ed.* **2020**, *59* (22), 8368–8392. https://doi.org/10.1002/anie.201911758.
(25) Penfold, N. J. W.; Yeow, J.; Boyer, C.; Armes, S. P. Emerging Trends in Polymerization-Induced Self-Assembly. *ACS Macro Lett* **2019**, *8* (8), 1029–1054. https://doi.org/10.1021/acsmacrolett.9b00464.
(26) Ng, G.; Yeow, J.; Xu, J.; Boyer, C. Application of Oxygen Tolerant PET-RAFT to Polymerization-Induced Self-Assembly. *Polym Chem* **2017**, *8* (18), 2841–2851. https://doi.org/10.1039/c7py00442g.
(27) Yeow, J.; Sugita, O. R.; Boyer, C. Visible Light-Mediated Polymerization-Induced Self-Assembly in the Absence of External Catalyst or Initiator. *ACS Macro Lett* **2016**, *5* (5), 558–564. https://doi.org/10.1021/acsmacrolett.6b00235.
(28) Cheng, Y. T.; Xia, Q.; Liu, H.; Solomon, M. B.; Brisson, E. R. L.; Blackman, L. D.; Ling, C. D.; Müllner, M. Tunable Polymer Nanoreactors from RAFT Polymerization-Induced Self-Assembly: Fabrication of Nanostructured Carbon-Coated Anatase as

Battery Anode Materials with Variable Morphology and Porosity. *ACS Appl Mater Interfaces* **2023**, *15* (9), 12261–12272. https://doi.org/10.1021/acsami.2c18928.
(29) Karagoz, B.; Esser, L.; Duong, H. T.; Basuki, J. S.; Boyer, C.; Davis, T. P. Polymerization-Induced Self-Assembly (PISA)-Control over the Morphology of Nanoparticles for Drug Delivery Applications. *Polym Chem* **2014**, *5* (2), 350–355. https://doi.org/10.1039/c3py01306e.
(30) Priester, A.; Yeng, J.; Zhang, Y.; Wang, R.; Convertine, A. J. PISA Printing from CTA Functionalized Polymer Scaffolds. *RSC Appl. Polymers* **2024**, *2* (4), 612–623. https://doi.org/10.1039/d3lp00252g.
(31) Phan, H.; Taresco, V.; Penelle, J.; Couturaud, B. Polymerisation-Induced Self-Assembly (PISA) as a Straightforward Formulation Strategy for Stimuli-Responsive Drug Delivery Systems and Biomaterials: Recent Advances. *Biomater Sci* **2021**, *9* (1), 38–50. https://doi.org/10.1039/D0BM01406K.
(32) Li, K.; Wang, Y.; Yang, G.; Byun, S.; Rao, G.; Shoen, C.; Yang, H.; Gulati, A.; Crick, D. C.; Cynamon, M.; Huang, G.; Docampo, R.; No, J. H.; Oldfield, E. Oxa, Thia, Heterocycle, and Carborane Analogues of SQ109: Bacterial and Protozoal Cell Growth Inhibitors. *ACS Infect Dis* **2015**, *1* (5), 215–221. https://doi.org/10.1021/acsinfecdis.5b00026.
(33) Wang, Z.; Yu, L.; Lv, C.; Wang, P.; Chen, Y.; Tang, X. Photoresponsive Cross-Linked Polymeric Particles for Phototriggered Burst Release. *Photochem Photobiol* **2013**, *89* (3), 552–559. https://doi.org/10.1111/php.12038.
(34) Lee, Y.; Boyer, C.; Kwon, M. S. Photocontrolled RAFT Polymerization: Past, Present, and Future. *Chem Soc Rev* **2023**, *52* (9), 3035–3097. https://doi.org/10.1039/D1CS00069A.
(35) McKenzie, T. G.; Da Costa, L. P. M.; Fu, Q.; Dunstan, D. E.; Qiao, G. G. Investigation into the Photolytic Stability of RAFT Agents and the Implications for Photopolymerization Reactions. *Polym Chem* **2016**, *7* (25), 4246–4253. https://doi.org/10.1039/c6py00808a.
(36) Sakellariou, G.; Siakali-Kioulafa, A.; Hadjichristidis, N. Synthesis, Chain Flexibility, and Glass-Transition Temperature of Poly (2,2-Diphenylethyl Methacrylate). *International Journal of Polymer Analysis and Characterization* **2003**, *8* (4), 269–277. https://doi.org/10.1080/10236660304881.
(37) Mandal, T. K.; Woo, E. M. Miscible Blends Comprising Two Carbonyl-Containing Polymers. Poly(ε-Caprolactone) with Poly(Benzyl Methacrylate). *Polym J* **1999**, *31* (3), 226–232. https://doi.org/10.1295/polymj.31.226.
(38) Kang, T. W.; Tamura, A.; Arisaka, Y.; Yui, N. Visible Light-Degradable Supramolecular Gels Comprising Cross-Linked Polyrotaxanes Capped with Trithiocarbonate Groups. *Polym Chem* **2021**, *12* (26), 3794–3805. https://doi.org/10.1039/d1py00569c.
(39) Akiba, I.; Sakurai, K. Characterizing Block-Copolymer Micelles Used in Nanomedicines via Solution Static Scattering Techniques. *Polym J* **2021**, *53* (9), 951–973. https://doi.org/10.1038/s41428-021-00489-9.